INTERNATIONAL JOURNAL FOR NUMERICAL METHODS IN FLUIDS
Int. J. Numer. Meth. Fluids 2000; **33**: 847–868

An adaptive boundary element approach to transient free surface flow as applied to injection molding

R. E. Khayat*,[1], W. Elsin and K. Kim

Department of Mechanical and Materials Engineering, The University of Western Ontario, London, Ontario, Canada N6A 5B9

SUMMARY

An adaptive (Lagrangian) boundary element approach is proposed for the general two-dimensional simulation of confined moving-boundary flow of viscous incompressible fluids. Only the quasi-steady creeping (Stokes) flow of a Newtonian fluid is examined. The method is stable as it includes remeshing capabilities of the deforming moving boundary, and thus it can handle large deformations. An algorithm is developed for mesh refinement of the deforming moving-boundary mesh. Several flow problems are presented to illustrate the utility of the approach, with particular emphasis on cavity filling and viscous fingering, as applied to conventional and gas-assisted injection molding. The accuracy of the method is assessed through the problem of jet flow and the transient fountain flow between two flat plates.

KEY WORDS: boundary element; molding; moving-boundary flow

1. INTRODUCTION

The numerical simulation of transient moving-boundary flow problems remains challenging despite the advent of powerful techniques. Typically, a boundary value problem of the moving type, which involves geometrical non-linearities, must be addressed. In contrast to conventional problems in fluid dynamics, the domain of computation, which is bounded in part by the moving boundary, is not known *a priori* since the shape of the moving boundary itself must be determined as part of the solution. A number of iterations are usually needed in order to reach the precise form of the moving boundary. The problem becomes even more challenging when, in addition, the shape of the moving boundary evolves with time, generating large distortions in the discretized domain of the fluid.

* Correspondence to: Department of Mechanical and Materials Engineering, The University of Western Ontario, London, Ontario, Canada N6A 5B9.
[1] E-mail: rkhayat@eng.uwo.ca

Received May 1999
Revised September 1999

Several numerical techniques have been developed for the solution of moving boundary/initial value problems. These techniques may be classified as Eulerian, Lagrangian, and mixed Eulerian–Lagrangian [1]. In the Eulerian description of the flow, the grid points remain stationary or move in a predetermined manner [2–5]. Typically, the fluid moves in and out of the computational cells. The method can handle arbitrarily large moving-boundary deformations without loss of accuracy. Its main disadvantage, however, is the lack of sharp definition of the moving boundary, and the consequent difficulty in imposing the kinematic and dynamic boundary conditions on the moving boundary. In the Lagrangian approach, the grid points move with local fluid particle [6–8]. The moving boundary is sharply defined and it is easy to impose the necessary boundary conditions. However, Lagrangian methods require mesh refinement or remeshing for large deformations of the moving boundary. Hybrid methods have also been developed, which combine the advantages of the Eulerian and Lagrangian methods [8]. Generally, an adaptive Lagrangian approach becomes difficult to implement when a volume method, such as the finite element method (FEM), is used. On the other hand, the boundary element method (BEM) is much easier to use along with adaptive remeshing as the dimension of the problem is reduced by one.

The BEM relates velocities at points within the fluid to the velocity and stress on the bounding surfaces. It is thus an ideal method for studying moving-boundary problems, where the velocity on the moving boundary is the quantity of prime interest. The advantages of the BEM include reduction of problem dimensionality, direct calculation of the interfacial velocity, the ability to track large surface deformations, and the potential for easy incorporation of interfacial tension as well as other surface effects.

The present paper is part of a series of studies on the applicability of the BEM to problems of the moving boundary type. Such problems include the planar deformation of a drop in a confined medium [9–11], gas-assisted injection molding [12], air venting during blow molding and thermoforming [13], and the transient mixing of Newtonian and viscoelastic fluids [14]. In particular, Khayat *et al*. [12] proposed an Eulerian BEM approach for free surface and interface problems. The approach is based on the discretization of the whole cavity similar to the FEM. In this case, the BEM loses its main advantage as a boundary-only method.

The present work addresses the numerical solution of a class of moving-boundary problems in a confined medium of the free surface type. An adaptive Lagrangian boundary element approach is adopted to determine the evolution of the moving boundary, taking advantage of the reduction by one dimension as a result of the boundary-only implementation. In this case, only the boundary is discretized. The formulation and numerical implementation are illustrated through problems in injection molding. Conventional injection molding is addressed by examining the filling stage by considering isothermal flow in a rectangular cavity with sudden expansion. Another variant of the process, namely gas-assisted injection molding, is also covered by examining the transient flow of a liquid inside a channel driven by gas pressure. The accuracy assessment of the method is addressed by studying the flow of a jet, and the transient fountain flow between two flat plates.

There is a number of simplifying assumptions that need to be made for the BEM to become applicable. The inherent transient nature of the flow process and the presence of a moving boundary make the simulation of the problem challenging because of the non-linearities involved [1]. The challenge becomes even greater if both inertia and viscoelastic (or, more

generally, non-Newtonian) effects are accounted for. Such non-linear phenomena have been addressed in moving-boundary problems with relevance to polymer processing. For instance, viscoelastic effects were examined on the growth of spherical and cylindrical shells of a fluid obeying a highly non-linear viscoelastic constitutive model [15]. It was found that, even under constant driving pressure, oscillatory growth results from elastic normal stress effects. In order to assess the mathematical intricacies in the case of pressure-driven flows, Khayat [16] examined the small planar deformation of a viscoelastic column of fluid obeying the upper-convected Maxwell fluid by applying a regular perturbation approach. It was found that the governing equations are indeed hyperbolic and therefore, unlike the Navier–Stokes equations, can entertain an oscillatory solution for a statically stressed fluid. The same problem was later examined for large deformations using the FEM [17]. Non-linear effects, such as those stemming from fluid elasticity, fluid inertia, and shear thinning, are difficult to account for in a boundary element approach despite the advent of recent techniques to handle non-linear and transient problems [18–21].

The paper is organized as follows. The problem formulation is presented in Section 2, where basic equations, the domain of computation, and boundary conditions are covered. The solution procedure, including the time marching scheme, adaptive meshing of the moving boundary(ies), determination of local curvature, and the contact problem are discussed in Section 3. Numerical assessment is covered in Section 4, while illustrative examples from conventional and gas-assisted injection molding are given in Section 5. Finally, concluding remarks are given in Section 6.

2. PROBLEM FORMULATION

In this section, the governing equations, domain description, and boundary conditions are reviewed together with some of the assumptions taken for the moving-boundary flow of viscous incompressible Newtonian fluids. Only low-Reynolds number flows, typically characterized by small velocities, small length scales, and/or high viscosity, will be considered. In this limit, the inertia terms in the momentum equation are negligible, so the flow is in a state of creeping motion. The formulation is thus limited to Stokes flow.

2.1. Governing equations

At any instant t, the fluid is assumed to occupy a two-dimensional region, $\Omega(t)$, which is bounded by $\Gamma(t)$. It is convenient to take $\Omega(t)$ as the inner domain, excluding $\Gamma(t)$. Thus, $\Omega(t) \cup \Gamma(t)$ constitutes the domain occupied by the fluid. The fluid is taken to be neutrally buoyant so the effects of gravity and any external body forces are negligible. The conservation of mass and linear momentum equations are given by

$$\nabla \cdot \mathbf{u}(\mathbf{x}, t) = 0, \qquad \nabla \cdot \boldsymbol{\sigma}(\mathbf{x}, t) = \mathbf{0}, \quad \mathbf{x} \in \Omega(t) \cup \Gamma(t) \tag{1}$$

where ∇ is the gradient operator, $\mathbf{x}$ is the position vector, $\mathbf{u}(\mathbf{x}, t)$ is the velocity vector, and $\boldsymbol{\sigma}(\mathbf{x}, t)$ is the total stress tensor given in terms of the hydrostatic pressure $p(\mathbf{x}, t)$ and excess

stress tensor $\boldsymbol{\tau}(\mathbf{x}, t)$. Here, $\boldsymbol{\sigma}(\mathbf{x}, t) = -p(\mathbf{x}, t)\mathbf{I} + \boldsymbol{\tau}(\mathbf{x}, t)$, where $\mathbf{I}$ is the unit tensor. In the present study, the fluid is assumed to be Newtonian, so that

$$\boldsymbol{\tau}(\mathbf{x}, t) = \mu \left\lfloor \nabla\mathbf{u}(\mathbf{x}, t) + \nabla\mathbf{u}^T(\mathbf{x}, t) \right\rfloor, \quad \mathbf{x} \in \Omega(t) \cup \Gamma(t) \tag{2}$$

where μ is the viscosity of the fluid. The superscript T denotes the transpose of the matrix. It is important to note that the acceleration term $\partial\mathbf{u}/\partial t$ in the momentum conservation equation has been neglected, so that for a Newtonian fluid, the formulation in question is not strictly unsteady, but quasi-steady. This quasi-steady state assumption is valid whenever $L^2/\nu \ll T$, where L and T are typical characteristic length and time of the flow, and $\nu = \mu/\rho$ is the kinematic viscosity (ρ being the density). In the present case, $T \sim L/U$, U being a typical value of the driving velocity, which can be related to the inlet flow rate in conventional injection molding, or the driving pressure drop in gas-assisted injection molding. Thus, for the quasi-steady state assumption to apply, one must have $UL/\nu \ll 1$. This is indeed typically the case for fluids of interest to mixing problems. Note also that this inequality is implied by the fact that the Reynolds number is small. Physically, the quasi-steady state approximation means that a Newtonian fluid immediately adjusts to changes in the movement of the boundary or boundary conditions.

2.2. Domain of computation of the moving-boundary problem

There are two classes of moving-boundary problems considered in this study, with direct relevance to conventional and gas-assisted injection molding. Each category of problem is illustrated in Figure 1. For conventional injection molding, Figure 1(a) illustrates the situation at a given time t. The boundary $\Gamma(t)$ is composed, at any time, of a part spanning the source region, Γ_s, the wetted part of the cavity, $\Gamma_w(t)$, and the moving front, $\Gamma_f(t)$. The wetted part of the cavity is taken to be time-dependent, as it grows as more fluid comes in contact with the wall. The overall boundary may thus be expressed as $\Gamma(t) = \Gamma_s \cup \Gamma_w(t) \cup \Gamma_f(t)$. The liquid occupying the domain $\Omega(t) \cup \Gamma(t)$ is called melt, in reference to polymeric liquids usually involved in injection molding processes.

The process of gas-assisted injection molding is illustrated in Figure 1(b). The real process consists of an initial stage of conventional injection molding, during which the melt is driven inside the cavity similarly to Figure 1(a). At some stage of the process, the melt stops being injected. Instead, the existing amount of liquid is driven by a gas, usually nitrogen, as depicted from Figure 1(b). Similar to conventional injection molding, there is a wetted part of the cavity, as well as a free surface (front), but there is no source of fluid. Instead, there is a moving (gas/melt) interface, $\Gamma_i(t)$. In this case, $\Gamma(t) = \Gamma_i(t) \cup \Gamma_w(t) \cup \Gamma_f(t)$. The driving pressure is assumed constant throughout the gas region. In principle, the motion of the gas must be accounted for, but, as a first approximation, it is neglected.

2.3. Boundary and initial conditions

While the boundary conditions on the source and wetted cavity are straightforward to implement, those on the melt front and gas/melt interface must be examined more closely. The velocity is assumed to be fully prescribed along the source boundary Γ_s. A general flow, $\mathbf{u}_s(\mathbf{x})$, usually a Poiseuille flow, is imposed

$$\mathbf{u}(\mathbf{x}, t) = \mathbf{u}_s(\mathbf{x}), \quad \mathbf{x} \in \Gamma_s \tag{3a}$$

If a gas/melt interface exists instead of a source, a driving (gas) pressure, Δp, is assumed to apply, such that the traction at the interface is given by

$$\mathbf{t}(\mathbf{x}, t) = -\Delta p \mathbf{n}(\mathbf{x}, t), \quad \mathbf{x} \in \Gamma_i(t) \tag{3b}$$

Here $\mathbf{t}(\mathbf{x}, t) = \boldsymbol{\sigma}(\mathbf{x}, t) \cdot \mathbf{n}(\mathbf{x}, t)$ is the traction, $\mathbf{n}$ is the normal unit vector at $\Gamma_i(t)$. Equation (3b) represents the dynamic condition at the interface. The fluid is assumed to adhere to the cavity boundary, so that stick and no-penetration boundary conditions apply on the wetted part of the cavity

$$\mathbf{u}(\mathbf{x}, t) = \mathbf{0}, \quad \mathbf{x} \in \Gamma_w(t) \tag{4}$$

The proper choice and implementation of a kinematic condition is generally not obvious [1].

The dynamic conditions on the free surface (melt front) are based on the continuity of the tangential stress (no traction) and discontinuity of normal stress caused by the interfacial tension

$$\mathbf{t}(\mathbf{x}, t) = \gamma \mathbf{n}(\mathbf{x}, t) \nabla \cdot \mathbf{n}(\mathbf{x}, t), \quad \mathbf{x} \in \Gamma_f(t) \tag{5}$$

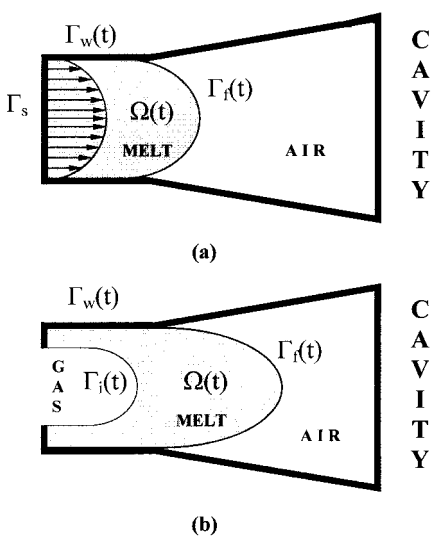

Figure 1. Schematic view and notations used for typical moving-boundary flows and confining cavity. Cavity filling or injection molding problems are typically illustrated in (a), while viscous fingering or gas-assisted injection molding problems are illustrated in (b).

where $\mathbf{n}$ is the normal vector outward to the front and γ is the surface tension coefficient. Note that boundary condition (5) is derived under conditions of equilibrium and uniform interfacial tension. Its validity under dynamic conditions is simply assumed [22,23]. The condition also assumes implicitly that the flow activity of the fluid outside the moving boundary (air) is negligible with the (atmospheric) pressure taken as zero.

In addition, the kinematic condition is needed, which relates the evolution of the moving boundary to the local velocity field. The moving boundary deforms in accordance with the instantaneous velocity field, thus determining new moving boundary positions with time. In a Lagrangian representation, the moving boundary is assumed to deform with the fluid velocity, such that the evolution of $\Gamma_f(t)$ or $\Gamma_i(t)$ is governed by the equation

$$\frac{d\mathbf{x}}{dt} = \mathbf{u}(\mathbf{x}, t), \quad \mathbf{x} \in \Gamma_f(t) \text{ or } \Gamma_i(t) \tag{6a}$$

Although easy to implement, the resulting scheme based on Equation (6a) tends to sweep points on the moving boundary along the tangent to the moving boundary, even if only small shape changes take place. Consequently, frequent redistribution of the moving boundary points or remeshing becomes necessary.

Alternatively, the moving boundary can be assumed to deform pointwise along the normal with the normal projection of the fluid velocity at the moving boundary [1]. This method keeps the points evenly distributed on the moving boundary. Thus, the following kinematic boundary condition results:

$$\frac{d\mathbf{x}}{dt} = \mathbf{n}(\mathbf{x}, t)[\mathbf{n}(\mathbf{x}, t) \cdot \mathbf{u}(\mathbf{x}, t)], \quad \mathbf{x} \in \Gamma_f(t) \text{ or } \Gamma_i(t) \tag{6b}$$

Unlike Equation (6a), the above equation prevents the nodes from being swept along the tangent to the moving boundary. However, it leads to numerical instability of the saw-tooth type. This difficulty is usually circumvented by applying a smoothing technique to the moving boundary. Given the remeshing capabilities of the present approach, the use of Equation (6a) turned out to be the good choice for the class of problems covered in this study.

As to the initial conditions, when the fluid assumed to be at rest initially

$$\mathbf{u}(\mathbf{x}, t = 0) \equiv \mathbf{0}, \quad \mathbf{x} \in \Omega(t = 0) \cup \Gamma(t = 0) \tag{7}$$

This is, however, not always the case. Sometimes a new flow configuration emerges out of an existing one that is not the equilibrium. This is illustrated in the viscous fingering problem.

Thus, the flow field is determined through the solution of Equations (1) and (2) subject to the initial condition (7) and the boundary conditions above using the boundary integral method.

2.4. Boundary integral equation

The general time-dependent integral equation for a moving domain is given by [24]

$$\int_{\Gamma(t)} \mathbf{t}(\mathbf{y}, t) \cdot \mathbf{J}(\mathbf{x}|\mathbf{y})\, \mathrm{d}\Gamma_{\mathbf{y}} - \int_{\Gamma(t)} \mathbf{n}(\mathbf{y}, t) \cdot [\mathbf{u}(\mathbf{y}, t) \cdot \mathbf{K}(\mathbf{x}|\mathbf{y})]\, \mathrm{d}\Gamma_{\mathbf{y}} = c(\mathbf{x}, t)\mathbf{u}(\mathbf{x}, t), \quad \mathbf{x} \in \Omega(t) \cup \Gamma(t) \tag{8}$$

Here $\mathbf{J}$ and $\mathbf{K}$ are the usual symmetric and anti-symmetric tensors with respect to $\mathbf{r} = \mathbf{x} - \mathbf{y}$, and are given as [24]

$$\mathbf{J}(\mathbf{x}|\mathbf{y}) = \frac{1}{4\pi}\left(\mathbf{I} \log r - \frac{\mathbf{rr}}{r^2}\right), \qquad \mathbf{K}(\mathbf{x}|\mathbf{y}) = -\frac{1}{\pi}\frac{\mathbf{rrr}}{r^4} \tag{9}$$

where $r = |\mathbf{r}|$. The function $c(\mathbf{x}, t)$, for $\mathbf{x} \in \Gamma(t)$, depends on the geometrical form of the boundary; its value arises from the jump in the value of the velocity integrals as the boundary is crossed. When the boundary is Lyapunov smooth, which requires that a local tangent to the moving boundary exists everywhere, the function $c(\mathbf{x}, t) = 1/2$. This is the case if constant boundary elements are used. Thus, the assumption of boundary smoothness is generally not valid in the vicinity of sharp corners, cusps or edges. In general, since $c(\mathbf{x}, t)$ depends solely on geometry, it may be evaluated assuming that a uniform velocity field, such as $\mathbf{u}(\mathbf{x}, t) = u\mathbf{e}$, is applied over the boundary, $\mathbf{e}$ being the direction of the velocity and u is its magnitude. Under these conditions, all derivatives (including tractions and stresses) must vanish. Hence, at any time t, Equation (8) reduces to

$$c(\mathbf{x}, t) = \int_{\Gamma(t)} \mathbf{n}(\mathbf{y}, t) \cdot [\mathbf{e} \cdot \mathbf{K}(\mathbf{x}|\mathbf{y}) \cdot \mathbf{e}]\, \mathrm{d}\Gamma_{\mathbf{y}}, \quad \mathbf{x} \in \Gamma(t) \tag{10}$$

Thus, at any time t, the form of the boundary $\Gamma(t)$ is determined, and the function $c(\mathbf{x}, t)$ is evaluated using the equation above.

3. SOLUTION PROCEDURE

In this section, a time marching scheme is proposed to discretize Equation (6). Once the flow field is determined at a given time step from Equation (8), the location of the moving boundary can be determined by solving Equation (6). As the boundary elements are distorted, the mesh is refined through element subdivision. The problem of contact between evolving moving boundary and surrounding cavity walls is finally covered.

3.1. Time marching scheme and moving boundary evolution

Consider now the application of the integral equation (8) for a point on the boundary, i.e., for $\mathbf{x} \in \Gamma(t)$. The discussion is limited to the case of conventional injection molding; the problem of gas-assisted injection molding is formulated in a similar manner. The flow field at any interior

point $\mathbf{x}\in\Omega(t)$ is obtained once the variables at the boundary are known. Since the velocity is fully prescribed on $\Gamma_s\cup\Gamma_w(t)$, only the traction (or stress) will be determined there. The traction is imposed on the moving boundary, $\Gamma_f(t)$, where the value of the velocity will be found. More explicitly, Equation (8) may be rewritten as

$$\int_{\Gamma_s\cup\Gamma_w(t)} \mathbf{t}(\mathbf{y},t)\cdot\mathbf{J}(\mathbf{x}|\mathbf{y})\,d\Gamma_y - \int_{\Gamma_f(t)} \mathbf{u}(\mathbf{y},t)\cdot[\mathbf{n}(\mathbf{y},t)\cdot\mathbf{K}(\mathbf{x}|\mathbf{y})]\,d\Gamma_y + \gamma\int_{\Gamma_f(t)} [\mathbf{n}(\mathbf{y},t)\nabla\cdot\mathbf{n}(\mathbf{y},t)]\cdot\mathbf{J}(\mathbf{x}|\mathbf{y})\,d\Gamma_y + \int_{\Gamma_s} \mathbf{u}_s(\mathbf{y})\cdot[\mathbf{n}(\mathbf{y})\cdot\mathbf{K}(\mathbf{x}|\mathbf{y})]\,d\Gamma_y = \begin{cases} c(\mathbf{x},t)\mathbf{u}_s(\mathbf{x}), & \mathbf{x}\in\Gamma_s \\ \mathbf{0}, & \mathbf{x}\in\Gamma_w(t) \\ c(\mathbf{x},t)\mathbf{u}(\mathbf{x},t), & \mathbf{x}\in\Gamma_f(t) \end{cases} \tag{11}$$

where conditions (3) and (4) are used. The unknowns in Equation (11) are thus $\mathbf{t}(\mathbf{x}\in\Gamma_s\cup\Gamma_w, t)$ and $\mathbf{u}(\mathbf{x}\in\Gamma_f, t)$, so that the values of the third and fourth integrals on the left-hand side are known.

The time derivative in Equation (6) is approximated by an explicit Eulerian finite difference scheme, with higher-order terms in the time increment Δt being neglected. The integral equation (10) relates the velocity and traction at the current time. Once the flow field is determined at each time step t, the position of the moving boundary is updated. The evolution of $\Gamma_f(t)$ is dictated by Equation (6). The updated position of the nodes that belong to the moving boundary is thus determined once the velocity at the moving boundary is obtained from the solution of Equation (11).

The integrals in Equation (11) are discretized into a finite sum of contributing terms over the boundaries. In this work, the boundary elements are assumed to be geometrically linear so that the velocity and traction are constant over each element. This makes the proposed adaptive remeshing method and estimation of curvature less difficult to implement since no interpolation of the flow variables is needed at each time step. The use of higher-order elements is possible, but may not be crucial given the mesh refinement and remeshing capabilities involved in the current procedure. The traction is constant over a flat linear element, and is multiply valued at a corner node if higher-order elements are used. In two dimensions, the traction is assumed to be double valued at every node of a curved boundary. Another advantage of the constant boundary element is that the value of $c(\mathbf{x}, t)$ is always and everywhere equal to $1/2$. In addition, the normal vector to each element is determined exactly.

3.2. Adaptive meshing

An algorithm is proposed for adaptive refinement of the mesh of the evolving moving boundary. Initially ($t<0$), the fluid is assumed to occupy a two-dimensional region, $\Omega_0 = \Omega(t=0)$, bounded by part of the cavity (source) and moving boundary. Typically, at $t\geq 0$, additional fluid penetrates Ω_0 (see Figure 1) and the volume starts to grow together with the boundary elements. At some point, some elements become too distorted, and mesh refinement

or remeshing is needed. Some other elements become too small, and adjacent segments need to be combined in this case.

The refinement is carried out by sub-dividing the elements that are too distorted, and combining elements that are too small. The criteria for sub-division and combination are based on the element length. In this case, at each time step of the flow, a list of elements is established, with the length of the segments greater than an imposed tolerance, $D_{\max}$. The list is sorted in order of increasing length of each element. In order to avoid generating mesh incompatibilities, larger elements are subdivided first. The sub-division starts from the last (i.e., the longest) element in the list, and is continued recursively until the list is empty. The sub-division is carried out by bisecting the element in the list.

When the distance between two nodes become smaller than an imposed minimum, $D_{\min}$, the segment in question is phased out, as it is combined with the two adjacent segments. The possibility for two nodes to become too close to each other arises when nodes are swept along the moving boundary. This situation is typical of free surface flow during the flow inside a channel or the filling of a cavity. The sweeping occurs as a result of the fountain flow effect at the moving boundary.

In summary, the first step in the adaptive meshing process consists of creating the data file containing the description of the problem domain, boundary conditions, loading, and initial mesh. The initial mesh is first examined to check for initially distorted elements. This mesh comes from a CAD system, such as PATRAN or PROENGINEER. The initial mesh is then refined by the adaptive remeshing scheme described above. The refined mesh is then submitted to the BEM solver. In practice, it is found that the quality of the initial mesh is adequate, and any initial refinement is not deemed necessary.

3.3. Determination of local curvature

The value of the curvature at a particular location (node or element) on the moving boundary is needed if surface tension is accounted for. The curvature is related to the divergence of the normal vector, $\mathbf{n}(x, y, z, t)$, at the location in question. Thus, the determination of the curvature is based on the estimation of the derivative of the normal vector components in the three directions. For this, it is convenient to define local co-ordinates (ξ, η) spanned by the tangent to the moving boundary at the local point and the normal to the boundary.

Consider now the curvature at an element (centroid) of the discretized boundary. The curvature is estimated directly at the centroid of the element rather than on a smooth interpolated boundary going through the element nodes. Boundary interpolation and fitting can be very costly. Generally, each node of the segment belongs to two elements, and the normal at the node is not uniquely defined. The normal vector is then taken as the segment average of the normal vectors to the elements to which the node belongs. The normal vector anywhere to the element, with nodes 1 and 2, may then be generally written as

$$\mathbf{n}(\mathbf{x}, t) = \sum_{i=1}^{2} \mathbf{n}_i(t)\phi_i[\xi(\mathbf{x}, t)] \tag{12}$$

where $\mathbf{n}_i(t)$ are the normal vectors at node i, and $\phi_i(\mathbf{x}, t)$ are suitably introduced interpolation functions. In this work, given the fact that linear elements are used, $\phi_i(\mathbf{x}, t)$ are taken to be linear. The partial derivatives of the normal vector are obtained by differentiating Equation (12). If the ξ co-ordinate axis is taken to lie along the element, then

$$\nabla \cdot \mathbf{n} = \frac{\partial n_\xi}{\partial \xi} \tag{13}$$

and the curvature is just given by $-\nabla \cdot \mathbf{n}/2$.

3.4. Contact between moving boundary and confining wall(s)

Initially, the fluid is assumed to occupy a prescribed area, Ω_0, which is taken as the starting step for the computation. Typically, Ω_0 is bounded by a source line, a part of the cavity, and the moving boundary. The source line is assumed to be part of the cavity at all times. The initial surface of fluid is thus in contact with the cavity only at the intersection of the moving boundary and the source line. The moving-boundary mesh is independent of the source surface mesh. The mesh of the source surface does not change with the subsequent motion. In fact the source line is part of the cavity, and its mesh coincides with that of the cavity.

The cavity walls are discretized into an appropriate number of elements that serve only to confine the fluid but do not come into the flow calculation. The number of cavity elements can thus be arbitrarily large, leading to an accurate representation of the cavity shape. This is particularly advantageous for practical situations where the geometry is typically complex. Obviously, the mesh density of the evolving moving boundary need not match that of the surrounding cavity. In other words, the accuracy in cavity representation is usually far superior to that of the surface bounding the moving fluid. A node or element that comes in contact with the wall is assumed to subsequently adhere to it. Contact is assumed to be established once the fluid has come close to the cavity wall to within a certain distance, which is usually taken to be of the order of an element size. The boundary conditions imposed at a given element depend on whether the element belongs to the moving boundary or the cavity.

4. NUMERICAL ASSESSMENT

The validity of the formulation and solution procedure is next demonstrated for a jet flow and the transient fountain flow between two flat plates. Ideally, comparison should be carried out between the numerical solution and an exact solution, including the interaction of the fluid with the surrounding cavity. But no analytical solution can be found for such cases. Comparison with existing formulations is also difficult; while some results exist for steady free surface flow, relatively little is reported for transient flows. However, some comparison will be carried out with existing finite element results for the flow between flat plates, as well as with experiments for the developing flow inside a tube.

4.1. Developing jet flow

Consider the jet flow of an incompressible viscous fluid occupying initially ($t < 0$) the space between two flat plates in the (x, y)-plane, i.e., a rectangular domain with $x \in [0, 3]$ and $y \in [0, 1]$ cm. At $t = 0$, Poiseuille flow is imposed at $x = 0$, with maximum velocity equal to 5 cm s^{-1}. The fluid emerges out of the channel at $x = 3$ cm. Because of the 'fountain flow' effect, a transverse velocity component exists, which leads to the swelling of the jet. Figure 2 shows the evolution of the jet at equal intervals of time over a period of 6 s. The figure is not drawn to scale for clarity. The jet has reached $x = 20$ cm, which is 17 times the width at the exit. The results in this case are based on $\Delta t = 0.01$ s, $D_{\max} = 0.2$ cm, and $D_{\min} = 0.1$ cm.

In order to assess the convergence of the method, several values of Δt have been used for fixed $D_{\max}$ and $D_{\min}$. Also, and more importantly, the influence of $D_{\max}$ is assessed for fixed time increments. It is found that when adaptive meshing is used, the influence of Δt is relatively insignificant on the evolution of error; this latter being effectively controlled by the value of $D_{\max}$ (and $D_{\min}$). The error is estimated by monitoring the evolution of the fluid volume during the flow relative to the amount of incoming fluid (flow rate) over time. The comparison is typically illustrated in Figure 3 for $D_{\max} \in [0.3, 2.5]$ cm, $D_{\min} = 0.1$ cm, and $\Delta t = 0.01$ s. The figure shows the evolution with time of the exact incoming flow volume, and that corresponding to the moving domain. Clearly, comparison improves as $D_{\max}$ decreases.

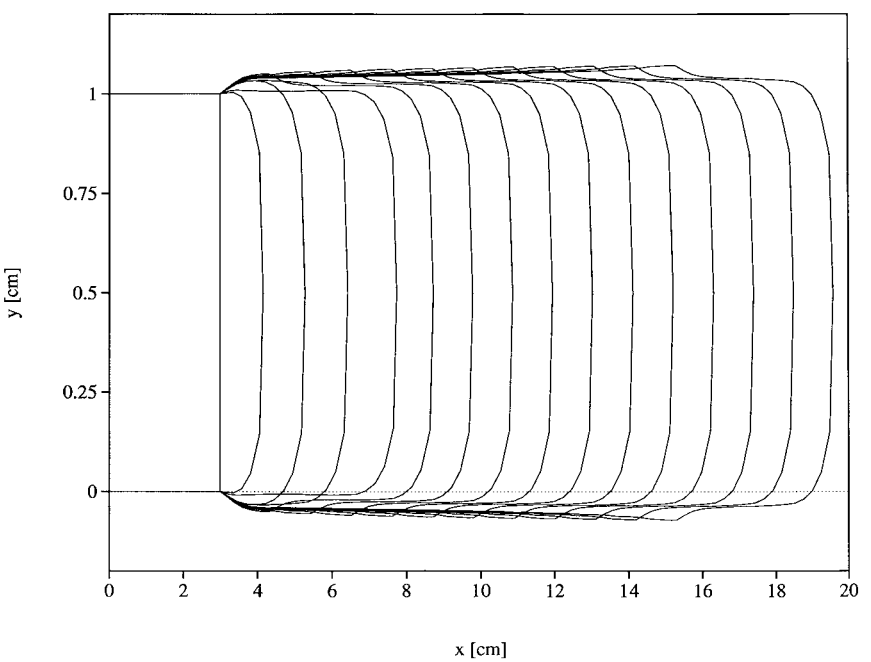

Figure 2. Simulation of an emerging jet. The fluid occupies the domain $(x, y) \in [0, 3] \times [0, 1]$ cm^2. Poiseuille flow is imposed at $x = 0$, with maximum velocity equal to 5 cm s^{-1}. The profile shown reflects the evolution of the jet over 4.5 s. Here $\Delta t = 0.01$ s.

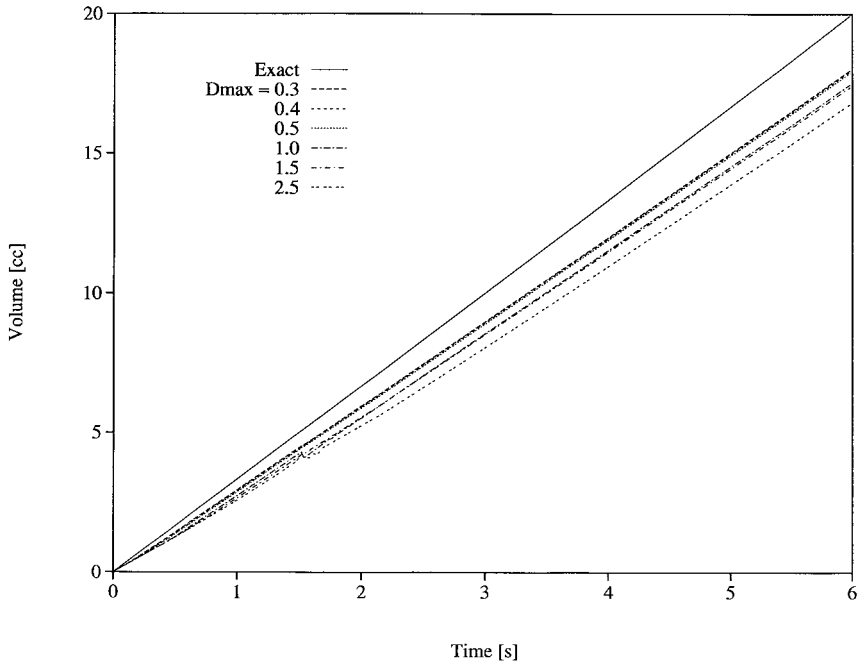

Figure 3. Influence of mesh size on numerical accuracy for the jet flow in Figure 2. The figure shows the evolution of the amount of outflow of fluid with time. Comparison shows the influence of $D_{\max}$ on error accumulation with time for $D_{\max} \in [0.3, 2.5]$ cm.

The evolution of the number of elements (segments) is also of interest. The results for the jet problem are shown in Figure 4 for $D_{\max} \in [0.3, \infty)$ cm, $D_{\min} = 0.1$ cm, and $\Delta t = 0.01$ s. Note that the limit $D_{\max} \to \infty$ corresponds to a fixed mesh. The figure indicates that the increase in the number of element is overall linear for any $D_{\max}$ value. In fact, the behavior is piecewise constant. This behavior is of course expected since the number of elements remains constant over intervals of time that decrease as $D_{\max}$ decreases.

4.2. Transient fountain flow between flat plates

The numerical implementation is further assessed by examining the start-up flow of a fluid between two flat plates, with a free front initially at rest. Gravity and surface tension effects are neglected, so that the free surface is initially flat and perpendicular to the walls (90° contact angle). These conditions correspond to the experiments of Behrens *et al.* [25] and the finite element calculations of Mavridis *et al.* [26]. For a typical boundary element simulation, the plates coincide with the $y = 0$ and $y = 1$ cm lines, and the domain occupied by the fluid is given by $(x, y) \in [0, 0.1] \times [0, 1]$ cm^2. Poiseuille flow is imposed at all times at $x = 0$, with a mean velocity equal to 1 cm s^{-1}. The boundary of the initial domain is subdivided into 40 elements (segments).

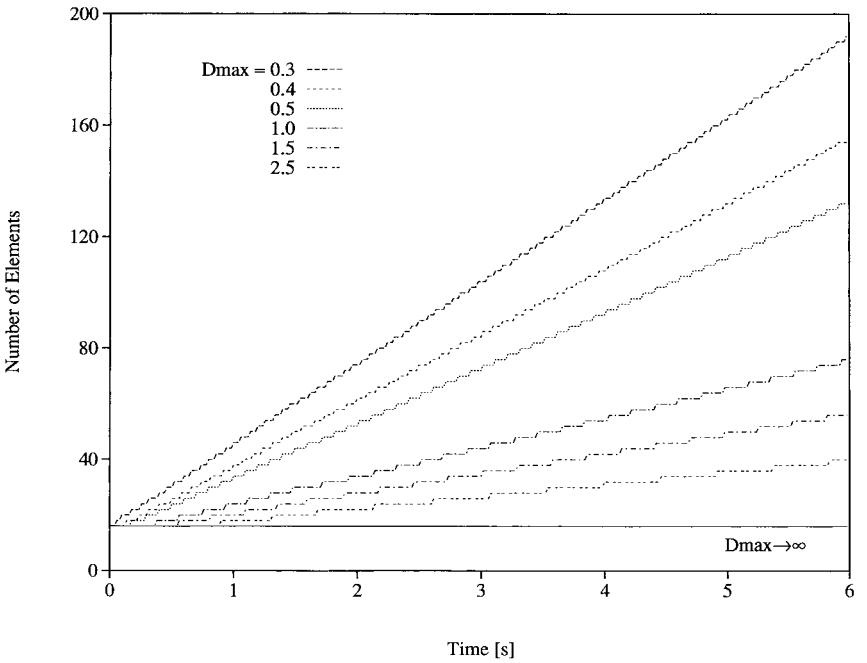

Figure 4. Influence of mesh size on the number of elements for the jet flow in Figure 2. The figure shows the evolution of the number of elements with time for $D_{max} \in [0.3, \infty)$ cm.

Figure 5 shows the evolution of the free surface shape. Steady state is reached in approximately 1.5 s, when the front tip, X_{max}, reaches 1.5 cm. At this stage the flow field remains invariant with respect to a frame of reference moving with average velocity of the fluid and the problem can be analyzed in the steady state [27]. The evolution of the number of elements for various values of D_{max} is shown in Figure 6. In this case, D_{min} is kept equal to 0.07 cm. Four values of D_{max} are considered in the range $[0.08, \infty)$. Again, when D_{max} is set equal to infinity, no element sub-division occurs. Unlike the case of jet flow, the number of elements is not linear with time.

Behrens *et al.* [25] performed experiments with Newtonian fluids in tubes. They monitored the evolution of the difference in tip and contact line positions, $X_{max} - X_{cl}$, as a function of tip position, X_{max}. A direct comparison with results based on the current formulation is of course impossible, but a qualitative comparison is possible. Figure 7 displays the dependence of $X_{max} - X_{cl}$ on X_{max} for three values of D_{max} (0.1–0.3 cm). There is a strong dependence on D_{max} when steady state is reached. All three curves exhibit fluctuation around the steady state level, which decreases as D_{max} decreases. There is also a strong overshoot for the cruder meshes. The results in the figure should be compared with those in Figure 6 of Reference [25].

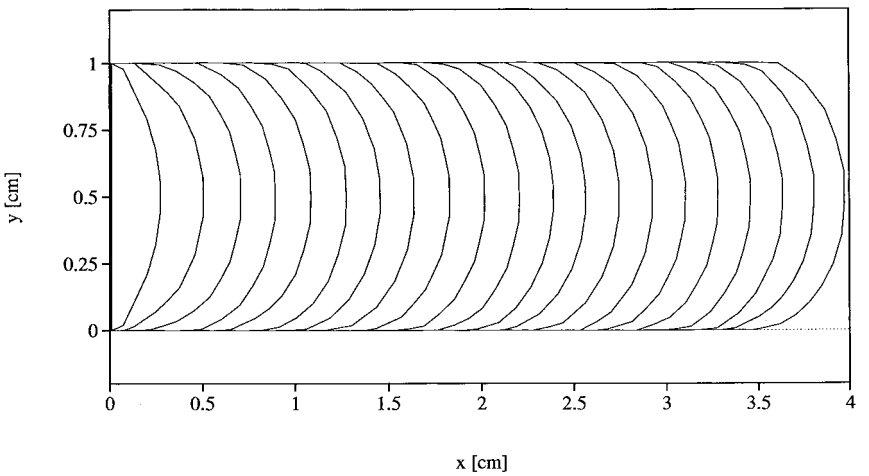

Figure 5. Transient fountain flow between flat plates. The fluid occupies initially the domain $(x, y) \in [0, 0.1] \times [0, 1]$ cm^2. Poiseuille flow is imposed at $x = 0$, with average velocity equal to 1 cm s^{-1}. The profile shown reflect the evolution of the flow over 4 s. Here $\Delta t = 0.01$ s.

5. ILLUSTRATIONS FROM INJECTION MOLDING

Elaborate numerical results are now presented for the developing flow between flat plates with viscous fingering. This problem is of relevance to the process of gas-assisted injection molding. Surface and interfacial tension effects as well as gravity are neglected. Another illustration is borrowed from conventional injection molding of a plate with sudden expansion.

5.1. Viscous fingering and gas-assisted injection molding

The potential of the proposed formulation and numerical implementation is now demonstrated for the transient problem of viscous fingering. This problem is of fundamental importance, and is also of significant practical interest as it is related to gas-assisted injection molding. This latter process is a variant of conventional injection molding. The process in fact consists of an initial phase when part of the cavity is filled similarly as in injection molding. Instead of filling the cavity (mold) entirely with liquid polymer, gas (usually nitrogen) is injected under pressure, which drives the melt further until it entirely fills the mold. The melt is left to cool and to solidify, resulting in a hollow molded product.

The processing sequence for gas-assisted injection molding is illustrated in Figure 8 for a flow between two flat plates. The initial stage consists of driving the melt during 0.02 s to fill the space roughly given by $(x, y) \in [0, 2] \times [0, 1]$ cm^2. During this time, Poiseuille flow is imposed at $x = 0$ with maximum velocity equal to 5 cm s^{-1}. At $t = 0.02$ s, gas is injected at $x = 0$, which becomes the sole fluid mover. At the gas/melt interface, a pressure of unit magnitude is applied, acting along the normal to the gas/melt interface (see Figure 1(b)). In

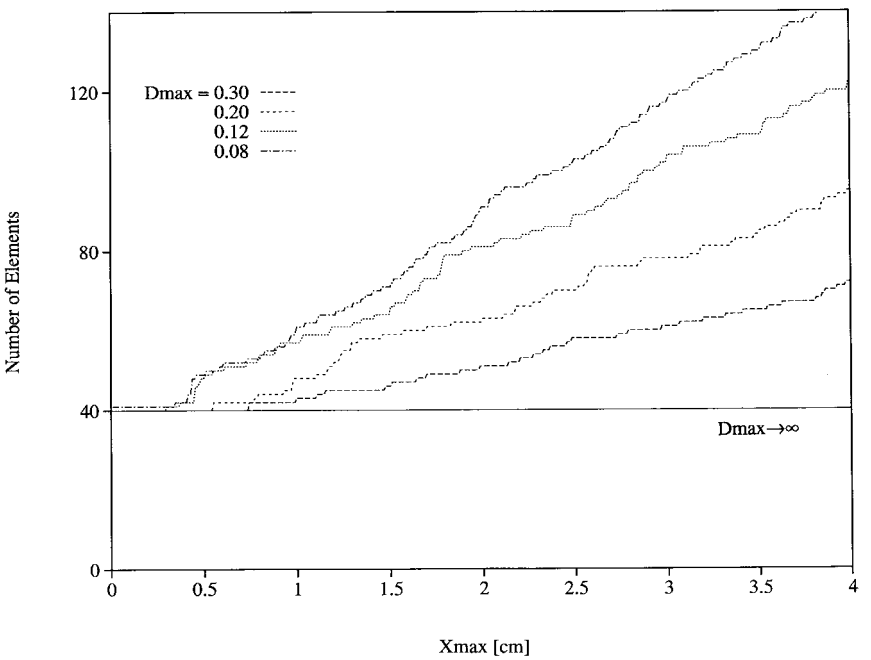

Figure 6. Influence of mesh size on the number of elements for the fountain flow in Figure 5. The figure shows the evolution of the number of elements with time.

this study, the pressure is maintained constant. The earlier stages corresponding to $t = 0.25$ and 0.44 s are typical of the process, when gas begins to penetrate the melt (fingering), with the melt adhering to the walls near the entrance.

The penetration proceeds further, with part of the melt literally swept away near the entrance; there is essentially no melt deposited at the entrance ($t > 0.4$ s). Instead, the melt is pushed forward to form a relatively thick layer along the wall of the entrance ($t = 0.67$ s). It is interesting to note that, near the entrance, there is a 'plug flow-like behavior', leaving a sharp cut in the melt. The amount of melt deposited along the wall increases with time, and the thickness is relatively constant for the most part behind the melt front ($t = 0.8$ s). Because of the melt deposition along the wall, the gas tip is constantly accelerating, eventually reaching the melt front ($t = 0.9$ s). At the same time, there is little flow activity upstream of the gas tip. The final stage in Figure 8 also shows that the gas tends to expand laterally as it is encountering less resistance near the melt front in the lateral direction(s). Finally, it is important to observe that the gas is bound to penetrate completely through the melt, a phenomenon known as 'blow-through' in the injection molding industry.

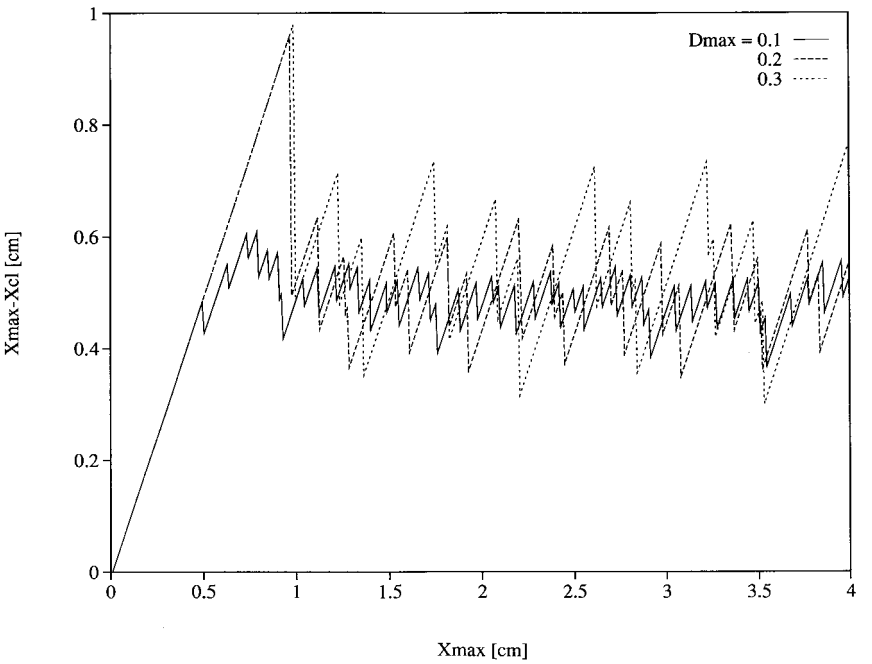

Figure 7. Dependence of $X_{\max} - X_{\mathrm{cl}}$ on front tip position, $X_{\max}$, for $D_{\max} \in [0.1, 0.3]$ cm.

5.2. Conventional injection molding

The final illustration presented in this study is borrowed from conventional injection molding. This process is complex as it involves flow, solidification, stress build-up, and warpage. The illustration here is limited to the filling stage of a rectangular cavity with sudden expansion. The fluid flows initially in a narrow section of the cavity occupying the region $(x, y) \in [0, 3] \times [0, 1]$ cm^2, and later into the larger square section $[3, 6] \times [-1, 2]$ cm^2, where the sudden expansion occurs. Initially, for $t < 0$, the fluid is assumed to occupy the region $[0, 0.1] \times [0, 1]$ cm^2 in the (x, y)-plane. The melt front is straight. At $t = 0$, Poiseuille flow is imposed at $x = 0$, corresponding to a maximum velocity equal to 5 cm s^{-1}. Throughout the calculation, Δt is equal to 0.0075 s, $D_{\max} = 0.18$ cm and $D_{\min} = 0.1$ cm. Approximately 600 steps are used for complete filling. Figure 9 displays the evolution of the flow for six different stages.

Figure 9 displays six typical stages of the filling process. Initially, and until approximately 0.04 s, the flow moves exactly as a transient fountain flow between two flat plates (Figure 5). This is illustrated in Figure 9 by the $t = 0.0375$ s stage. Once the fluid emerges into the square section, the flow behaves like the jet problem in Figure 2. This situation is clearly shown for $t = 0.0975$ s. The fluid comes in contact with the cavity wall at $x = 6$ cm, at approximately $t = 0.11$ s. At this stage, the swelling in the jet increases as shown typically in the figure for $t = 0.1275$ s. It is interesting to observe that the jet at this stage, despite the pronounced

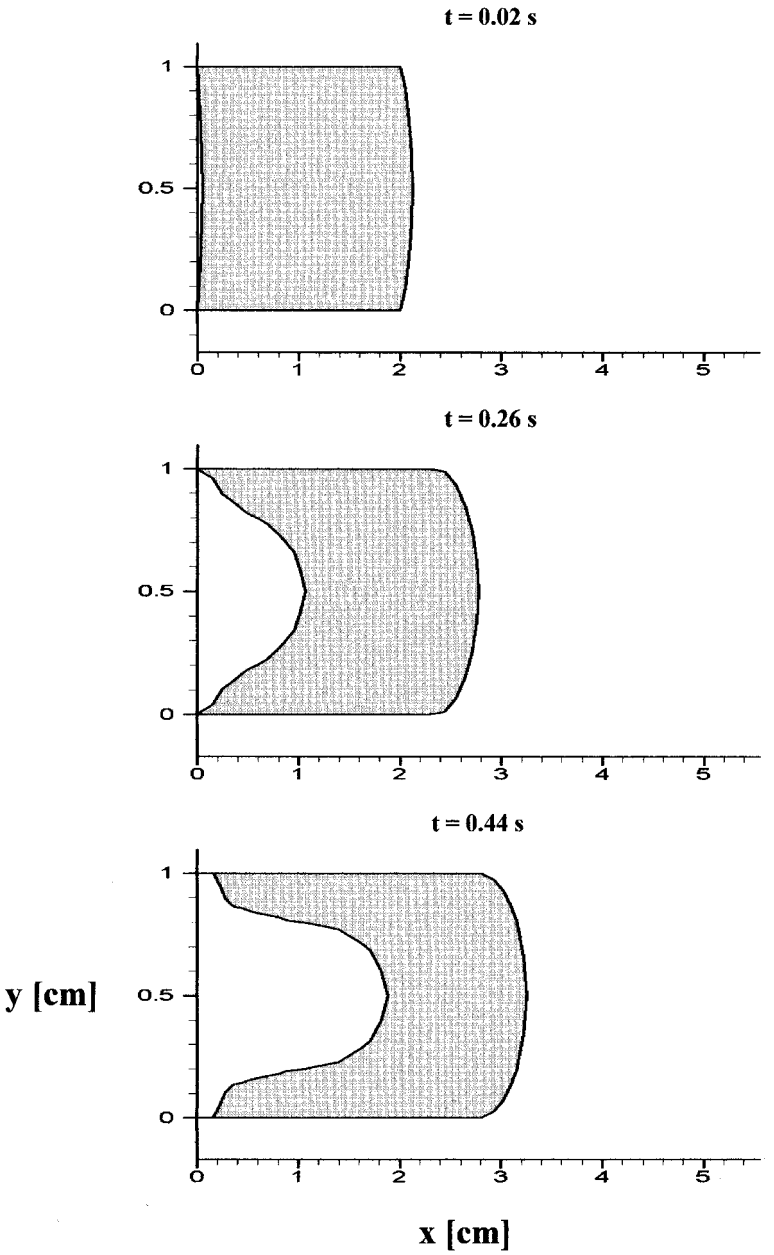

Figure 8. Viscous fingering and its relevance to gas-assisted injection molding. The figure shows six stages fot $0 < t$ [s] < 1, for $\Delta t = 0.001$ s, $D_{\max} = 0.1$ cm.

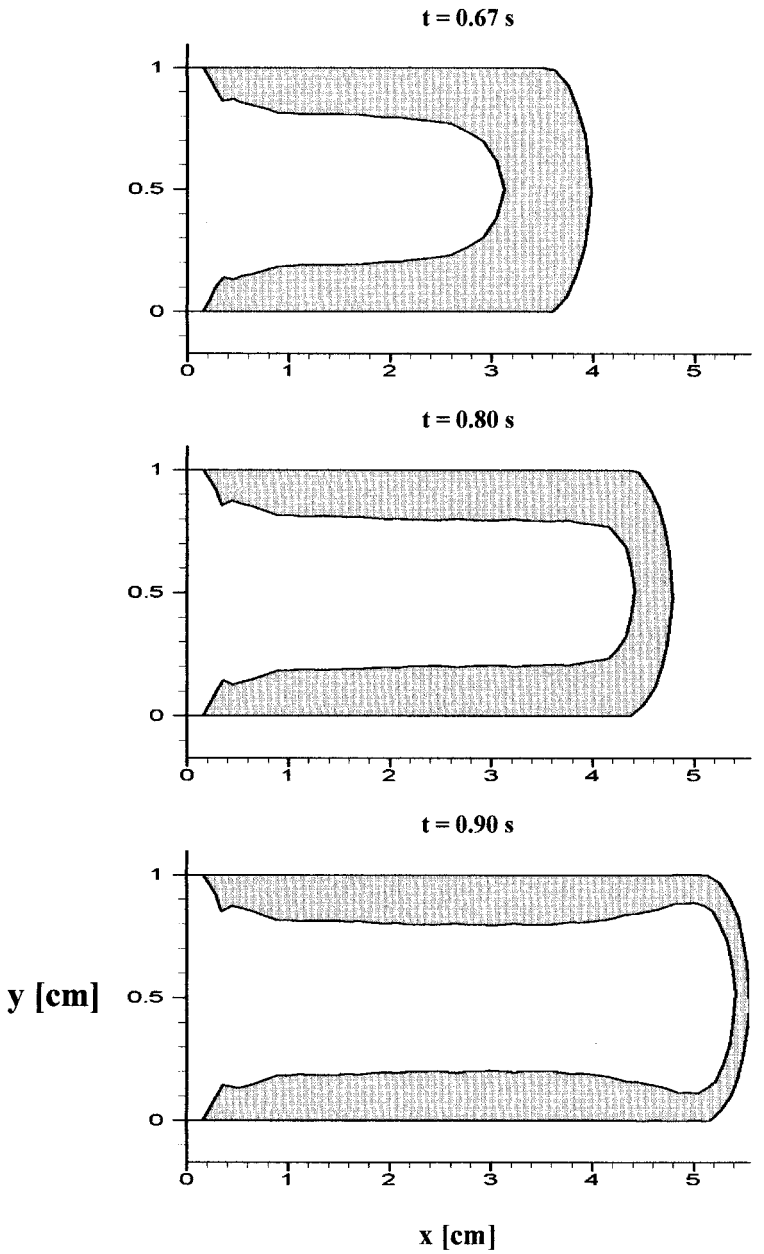

Figure 8 (*Continued*)

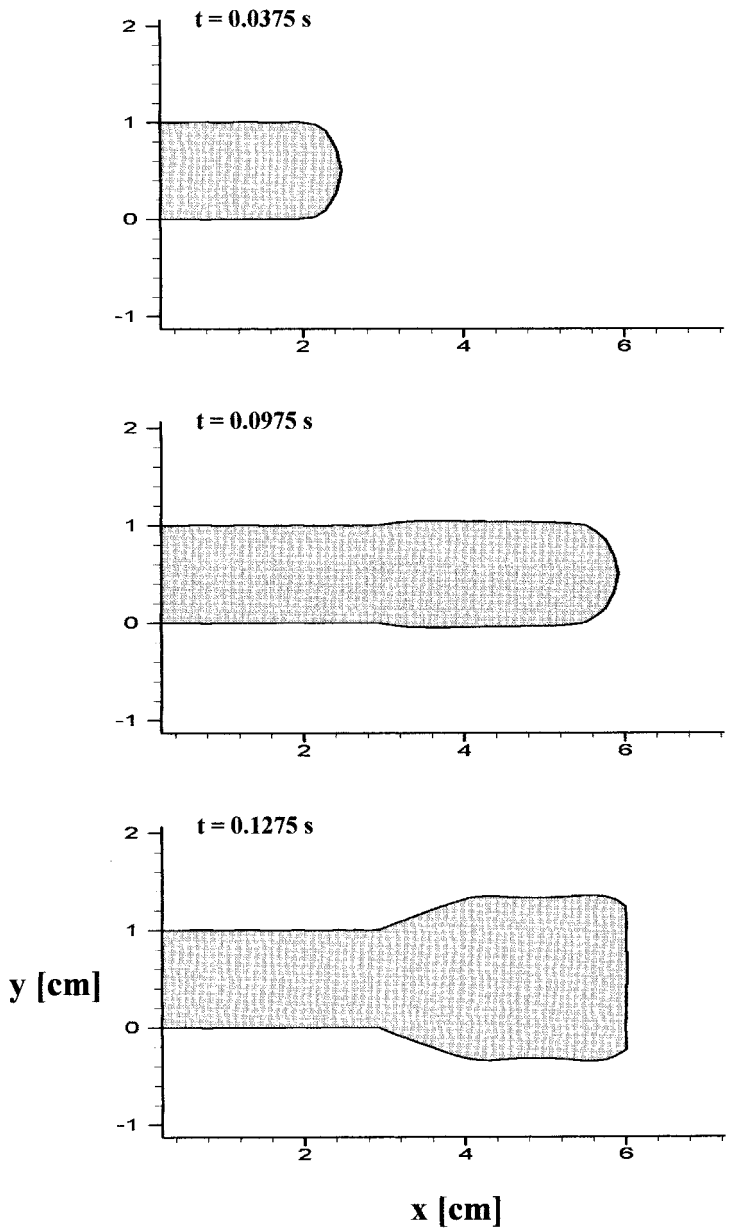

Figure 9. Conventional injection molding in a rectangular cavity with sudden expansion. The figure shows six stages fot $0 < t$ [s] < 0.23, for $\Delta t = 0.0075$ s, $D_{\max} = 0.1$ cm.

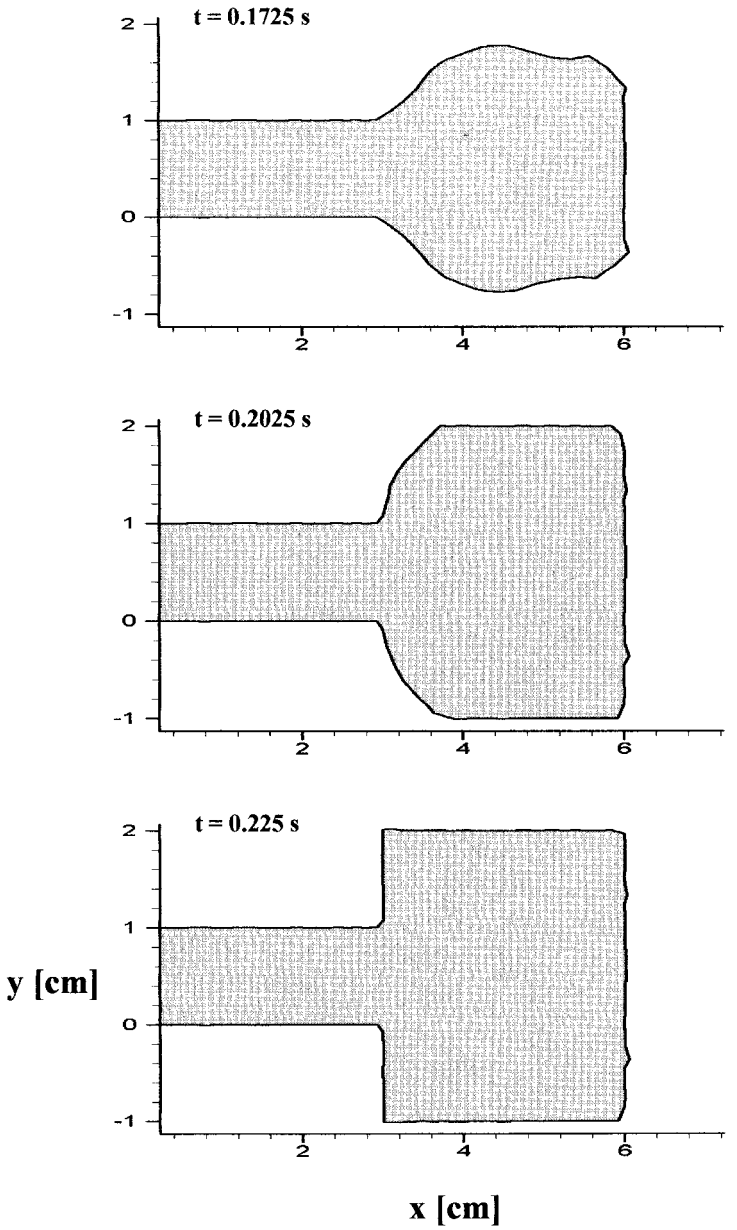

Figure 9 (*Continued*)

amount of swelling, still exhibits straight (horizontal) sides between 4 and 6 cm and the (vertical) wall, and tapers linearly between 3 and 4 cm.

As the flow continues, the swelling becomes less uniform as depicted at $t = 0.1725$ s. There is more swelling further upstream from and a slight depression near the wall ($x = 6$ cm). It is noted that symmetry is essentially preserved. The $t = 0.2025$ s stage reflects typically the stage when the fluid has come in contact in the lateral walls. In this case, there remains only one part of the melt front that is still free to move, between 3 and 3.6 cm. Two small protrusions into the $x > 6$ cm range are also shown, which can be controlled (eliminated) by decreasing the time increment. Note that at this stage, the walls at $x = 3$ cm have not been wetted yet. Finally, at $t = 0.225$ s, the cavity is completely filled.

6. CONCLUSION

An adaptive Lagrangian boundary element approach is proposed for the flow of Newtonian viscous fluids. The mesh refinement algorithm is simple and yet is found to be robust and suitable for moving boundary flow. The convergence and accuracy of the numerical implementation are assessed for the problem of jet flow, and the transient fountain flow between flat plates. The method is illustrated through the problem of viscous fingering in a channel, with relevance to gas-assisted injection molding, and the filling stage of injection molding inside a rectangular cavity with sudden expansion.

ACKNOWLEDGMENTS

The funding of this study has been provided by the Natural Sciences and Engineering Council of Canada, which is gratefully acknowledged.

REFERENCES

1. Floryan JM, Rasmussen H. Numerical methods for viscous flows with moving boundaries. *Applied Mechanics Reviews* 1989; **42**: 323.
2. Nickell RE, Tanner RI, Caswell B. The solution of viscous incompressible jet and free-surface flows using finite element method. *Journal of Fluid Mechanics* 1974; **65**: 189.
3. Siliman WJ, Scriven LE. Separating flow near a static contact line: slip at a wall and shape of a free surface. *Journal of Computational Physics* 1980; **34**: 287.
4. Ruschak KJ. A method of incorporating free boundaries with surface tension in finite element fluid flow simulation. *International Journal for Numerical Methods in Engineering* 1980; **15**: 639.
5. Kawahara M, Miwa T. Finite element analysis of wave motion. *International Journal for Numerical Methods in Engineering* 1984; **20**: 1193.
6. Bach P, Hassager O. An algorithm for the use of the Lagrangian specification in Newtonian fluid mechanics and applications to free surface flows. *Journal of Fluid Mechanics* 1985; **152**: 173.
7. Ramaswany B, Kawahara M. Lagrangian finite element analysis applied to viscous free surface fluid flow. *International Journal for Numerical Methods in Fluids* 1987; **7**: 953.
8. Chipada S, Jue TC, Joo SW, Wheeler MF, Ramaswamy R. Numerical simulation of free-boundary problems. *Computational Fluid Dynamics* 1996; **7**: 91.
9. Khayat RE, Luciani A, Utracki LA. Boundary-element analysis of planar drop deformation in confined flow. Part I. Newtonian fluids. *Engineering Analysis with Boundary Elements* 1997; **19**: 279.
10. Khayat RE, Huneault M, Utracki LA, Duquette R. A boundary element analysis of planar drop deformation in the screw channel of a mixing extruder. *Engineering Analysis with Boundary Elements* 1998; **21**: 155–168.

11. Khayat RE. Boundary-element analysis of planar drop deformation in confined flow. Part II. Viscelastic fluids. *Engineering Analysis with Boundary Elements* 1998; **22**: 291.
12. Khayat RE, Derdouri A, Hebert LP. A boundary element approach to three-dimensional gas-assisted injection molding. *Journal of Non-Newtonian Fluid Mechanics* 1995; **57**: 253.
13. Khayat RE, Raducanu P. A coupled finite element/boundary element approach for the three-dimensional simulation of air venting in blow molding and thermoforming. *International Journal for Numerical Methods in Engineering* 1998; **43**: 151.
14. Khayat RE, Derdouri A, Frayce D. Boundary element analysis of three-dimensional transient mixing processes of Newtonian and viscoelastic fluids. *International Journal for Numerical Methods in Fluids* 1998; **28**: 815.
15. Khayat RE, Garcia-Rejon A. Uniaxial and biaxial unsteady inflation of a viscoelastic material. *Journal of Non-Newtonian Fluid Mechanics* 1992; **43**: 31.
16. Khayat RE. A perturbation approach to planar flow of a viscoelastic fluid with two moving free boundaries. *Quarterly Journal of Mechanics and Applied Mathematics* 1994; **47**(3): 342.
17. Mao W, Khayat RE. Numerical simulation of transient planar flow of a viscoelastic materials with two moving free surfaces. *International Journal for Numerical Methods in Fluids* 1995; **21**: 1137.
18. Wrobel LC. The dual reciprocity boundary element formulation for nonlinear problems. *Computational Methods and Applications in Mechanical Engineering* 1987; **65**: 147.
19. Nowak AJ. Application of the multiple reciprocity method for solving nonlinear problems. In *Advanced Computational Methods in Heat Transfer II*, *Vol I: Conduction*, *Radiation and Phase Change*, Wrobel LC, Brebbia CA, Nowak AJ (eds). Computational Mechanics Publications: New York, 1995.
20. Neves AC, Brebbia CA. The multiple reciprocity boundary element method for transforming domain integrals to the boundary. *International Journal for Numerical Methods in Engineering* 1991; **31**: 709.
21. Frayce D, Khayat RE. A dual reciprocity boundary element approach to three-dimensional transient heat conduction as applied to materials processing. *Numerical Heat Transfer A* 1996; **29**: 243.
22. Batchelor GK. *Introduction to Fluid Dynamics*. Cambridge University Press: Cambridge, 1967.
23. Park WC, Homsy GM. Two-phase displacement in Hele–Shaw cells: theory. *Journal of Fluid Mechanics* 1984; **139**: 291.
24. Brebbia CA, Dominguez J. *Boundary Elements: An Introductory Course*. Computational Mechanics Publications and McGraw-Hill: New York, 1992.
25. Behrens RA, Crochet MJ, Denson CD, Metzner AB. Transient free-surface flows: Motion of a fluid advancing in a tube. *American Institute of Chemical Engineering Journal* 1987; **33**: 1178.
26. Mavridis H, Hrymak AN, Vlachopoulos J. Transient free-surface flows in injection mold filling. *American Institute of Chemical Engineering Journal* 1988; **34**: 403.
27. Mavridis H, Hrymak AN, Vlachopoulos J. Finite-element simulation of fountain flow in injection molding. *Polymer Engineering Science* 1986; **26**: 410.

